Symmetry breaking in symmetric and asymmetric double-well potentials

G. Theocharis,[1] P. G. Kevrekidis,[2] D. J. Frantzeskakis,[1] and P. Schmelcher[3,4]
[1]*Department of Physics, University of Athens, Panepistimiopolis, Zografos, Athens 157 84, Greece*
[2]*Department of Mathematics and Statistics, University of Massachusetts, Amherst, Massachusetts 01003-4515, USA*
[3]*Theoretische Chemie, Physikalisch-Chemisches Institut, INF 229, Universität Heidelberg, 69120 Heidelberg, Germany*
[4]*Physikalisches Institut, Philosophenweg 12, Universität Heidelberg, 69120 Heidelberg, Germany*
(Received 22 March 2006; revised manuscript received 11 July 2006; published 20 November 2006)

Motivated by recent experimental studies of matter waves and optical beams in double-well potentials, we study the corresponding solutions of the nonlinear Schrödinger equation. Using a Galerkin-type approach, we obtain a detailed handle on the nonlinear solution branches of the problem, starting from the corresponding linear ones, and we predict the relevant bifurcations for both attractive and repulsive nonlinearities. The dynamics of the ensuing unstable solutions is also examined. The results illustrate the differences that arise between the steady states and the bifurcations emerging in symmetric and asymmetric double wells.

DOI: 10.1103/PhysRevE.74.056608 PACS number(s): 42.65.Wi, 42.65.Tg, 03.65.Ge, 03.75.Lm

I. INTRODUCTION

It is well known that the nonlinear Schrödinger (NLS) equation is a fundamental model describing the evolution of a complex field envelope in nonlinear dispersive media [1]. As such, it plays a key role in many different contexts, ranging from nonlinear and atom optics to plasma physics, fluid, and even biophysical models [2]. Interest in the NLS equation has dramatically increased during the past few years, as it also describes the mean-field dynamics of Bose-Einstein condensates (BECs) [3]. In this context, the NLS is also known as the Gross-Pitaevskii (GP) equation, and typically incorporates external potentials that are used for the BEC confinement. Such potentials may be, e.g., harmonic (implemented by, e.g., external magnetic fields) or periodic (implemented by the interference of laser beams), so-called optical lattices [4]. Importantly, NLS models with similar external potentials appear also in the context of optics, where they respectively describe the evolution of an optical beam in a graded-index waveguide or in periodic waveguide arrays [5,6].

Another type of external potential, which has mainly been studied theoretically in the BEC context [7–12], is the double-well potential. Moreover, it has been demonstrated experimentally that a BEC either tunnels and performs Josephson oscillations between the wells, or is subject to macroscopic quantum self-trapping [13]. On the other hand, in the context of optics, a double-well potential can be created by a two-hump self-guided laser beam in Kerr media [14]. A different alternative was offered in Ref. [15], wherein the first stages of the evolution of an optical beam, initially focused between the wells of a photorefractive crystal, were monitored.

One of the particularly interesting features of either matter waves or optical beams in double-well potentials is the *spontaneous symmetry breaking*, i.e., the localization of the respective order parameter in one of the wells of the potential. Symmetry breaking solutions of the NLS model have first been predicted in the context of molecular states [16] and, apart from the physical contexts of BECs [7–12] (see also Ref. [17]) and optics [14,15,18] mentioned above, they have also been studied from a mathematical point of view in Refs. [19–21].

These works underscore the relevance and timeliness of a better understanding of the dynamics of nonlinear waves in double-well potentials. Such studies are particularly interesting and important not only from a fundamental viewpoint, but also for applications. To make our point stronger, we note that double-well potentials have been used in recent BEC experiments dealing with matter-wave interferometers [22] and noise thermometry [23]. In view of the above, in the present work we offer a systematic methodology, based on a two-mode expansion, of how to tackle problems in double wells, with regard to their stationary states, as well as the bifurcations (and ensuing instabilities) that arise in them. This methodology can be used not only for symmetric double wells (see, e.g., Refs. [15,20]) but also asymmetric ones (weak asymmetries may easily be introduced in experimental situations, as is explained below). This way, considering both cases of attractive and repulsive nonlinearities, we illustrate the ways in which a symmetric double-well potential is different from an asymmetric one. In particular, we demonstrate that, contrary to the case of symmetric potentials where symmetry breaking follows a pitchfork bifurcation, in asymmetric double wells the bifurcation is of the saddle-node type. Although this result is expected from general bifurcation theory [24], the proposed methodology is able not only to identify the nonlinear states stemming from the linear ones, but also to calculate accurately the bifurcation points (in both cases of symmetric and asymmetric double wells, and for attractive and repulsive nonlinearities).

The paper is structured as follows. In Sec. II, we present the model and set up the analytical framework. In Sec. III, we illustrate the value of the method by highlighting the significant differences of symmetric and asymmetric double wells. In Sec. IV, we examine the dynamics of the obtained unstable solutions. Finally, in Sec. V, we summarize our findings and discuss future directions.

II. MODEL AND ANALYTICAL APPROACH

In a quasi-1D setting, the evolution of the mean-field wave function of a BEC [4] (or the envelope of an optical

beam [5]) is described by the following normalized NLS (GP) equation:

$$i\partial_t u = -\frac{1}{2}\partial_x^2 u + s|u|^2 u + V(x)u - \mu u. \tag{1}$$

In the BEC (optics) context, μ denotes the chemical potential (propagation constant) and $s=\pm 1$ is used for repulsive or attractive interatomic interactions (defocusing or focusing Kerr nonlinearity), respectively; below, for simplicity, we will adopt the terms attractive and repulsive nonlinearity for $s=\pm 1$, respectively. Finally, in Eq. (1), $V(x)$ is the double-well potential, which is assumed to be composed by a parabolic trap (of strength Ω) and a sech^2-shaped barrier (of strength V_0, width w, and location x_0); in particular, $V(x)$ is of the form

$$V(x) = \frac{1}{2}\Omega^2 x^2 + V_0\,\mathrm{sech}^2\left(\frac{x-x_0}{w}\right), \tag{2}$$

with the choice $x_0=0$ ($x_0\neq 0$) corresponding to a symmetric (asymmetric) double well. Note that such a double well can be implemented in BEC experiments upon, e.g., combining a magnetic trap with a sharply focused, blue-detuned laser beam [25]. Similar double wells can also be implemented, e.g., in optical systems.

The spectrum of the underlying linear Schrödinger equation ($s=0$) consists of a ground state, $u_0(x)$, and excited states, $u_l(x)$ ($l\geqslant 1$). In the *weakly nonlinear regime* of the nonlinear problem, using a Galerkin-type approach, we expand $u(x,t)$ as

$$u(x,t) = c_0(t)u_0(x) + c_1(t)u_1(x) + \cdots, \tag{3}$$

and truncate the expansion, keeping solely the first two modes; here $c_{0,1}(t)$ are unknown time-dependent complex prefactors. Once again, it is worth noticing that such an approximation (involving the truncation of higher-order modes and the spatio-temporal factorization of the wave function) is expected to be quite useful for a weakly nonlinear analysis, i.e., for a sufficiently small L^2 norm (or, physically speaking, number of particles—see also below) of the solution. In fact, as will be seen below, we will be able to identify the nonlinear states that stem from the linear ones, as well as their bifurcations.

Substituting Eq. (3) into Eq. (1), and projecting the result to the corresponding eigenmodes, we obtain the following ordinary differential equations (ODEs), for the projections to u_0 and u_1, respectively:

$$\begin{aligned} i\dot{c}_0 &= (\omega_0-\mu)c_0 + sA_0|c_0|^2c_0 + sB(2|c_1|^2c_0 + c_1^2\bar{c}_0), \\ &\quad + s\Gamma_1|c_1|^2c_1 + s\Gamma_0(2|c_0|^2c_1 + c_0^2\bar{c}_1), \end{aligned} \tag{4}$$

$$\begin{aligned} i\dot{c}_1 &= (\omega_1-\mu)c_1 + sA_1|c_1|^2c_1 + sB(2|c_0|^2c_1 + c_0^2\bar{c}_1), \\ &\quad + s\Gamma_0|c_0|^2c_0 + s\Gamma_1(2|c_1|^2c_0 + c_1^2\bar{c}_0). \end{aligned} \tag{5}$$

In Eqs. (4) and (5), dots denote time derivatives, overbars denote complex conjugates, $\omega_{0,1}$ are the eigenvalues corresponding to the eigenstates $u_{0,1}$, while $A_0=\int u_0^4 dx$, $A_1=\int u_1^4 dx$, $B=\int u_0^2 u_1^2 dx$, $\Gamma_1=\int u_0 u_1^3 dx$, and $\Gamma_0=\int u_1 u_0^3 dx$ are constants. Recall that u_0 and u_1 are real (due to the Hermitian nature of the underlying linear Schrödinger problem) and are also orthonormal. Notice also that in the symmetric case ($x_0=0$), due to the parity of the eigenfunctions, the constants $\Gamma_0=\Gamma_1=0$.

We now use amplitude-phase (action-angle) variables, $c_j=\rho_j e^{i\phi_j}$, $j=0,1$ (ρ_j and ϕ_j are assumed to be real), to derive from the ODEs (4) and (5) a set of four equations. Introducing the function $\varphi\equiv\phi_1-\phi_0$, we find that the equations for ρ_0 and ϕ_0 are

$$\dot{\rho}_0 = s[(\Gamma_0\rho_0^2 + \Gamma_1\rho_1^2)\rho_1\sin(\varphi) + B\rho_1^2\rho_0\sin(2\varphi)], \tag{6}$$

$$\begin{aligned} \dot{\phi}_0 &= (\mu-\omega_0) - sA_0\rho_0^2 - 2sB\rho_1^2 - sB\rho_1^2\cos(2\varphi) \\ &\quad - s\left(\frac{\Gamma_1\rho_1^3}{\rho_0} + 3\rho_0\rho_1\Gamma_0\right)\cos(\varphi), \end{aligned} \tag{7}$$

while the equations for ρ_1,ϕ_1 are found by interchanging indices 1 and 0 in the above equations. Next, taking into consideration the conservation of the squared (L^2) norm $N=\int|u|^2dx$ [which is an integral of motion of Eq. (1) describing the number of particles in BECs or the power in optics], we obtain the equation $\rho_0^2+\rho_1^2=N$. Finally, subtracting Eq. (7) for $\dot{\phi}_0$, from the corresponding one for $\dot{\phi}_1$, we obtain

$$\begin{aligned} \dot{\varphi} &= -\Delta\omega + s(A_0\rho_0^2 - A_1\rho_1^2) - sB[2+\cos(2\varphi)](\rho_0^2-\rho_1^2) \\ &\quad - s\frac{\cos(\varphi)}{\rho_0\rho_1}\times[\Gamma_0\rho_0^2(\rho_0^2-3\rho_1^2) + \Gamma_1\rho_1^2(3\rho_0^2-\rho_1^2)]. \end{aligned} \tag{8}$$

Equations (6) and (8) constitute a dynamical system, which, in principle, can be thoroughly investigated using phase-space analysis (such an approach has been presented in Refs. [7,8] for similar systems that were derived using a different expansion of the field u). Here, we will focus on the fixed points of the system [corresponding to the nonlinear eigenstates of Eq. (1)], and analyze their stability and bifurcations.

III. BIFURCATIONS AND STABILITY ANALYSIS

Below, we will analyze all possible cases ($s=\pm 1$, $x_0=0$, $x_0\neq 0$) for the double well of Eq. (2) with $V_0=1$, $\Omega=0.1$, and $w=0.5$ (the results do not change qualitatively using different values for these parameters).

A. Symmetric double well

First we consider the case of a symmetric double-well potential, i.e., $x_0=0$. The form of the double-well potential, as well as the eigenvalues, the ground state u_0, and the first excited state u_1 of the corresponding linear problem ($s=0$), are shown in Fig. 1. In this case, the parameters involved in Eqs. (6) and (8) are found to be $A_0=0.090\,78$, $A_1=0.095\,02$, $B=0.089\,64$, $\omega_0=0.132\,82$, and $\omega_1=0.155\,71$. Recall that because of the even and odd parity of the linear states u_0, u_1, we have $\Gamma_0=\Gamma_1=0$.

Since we are interested in real solutions of Eq. (1), we will confine our considerations to steady states with $\varphi=0$ (mod π) [note that, as observed from Eq. (3), one can realize

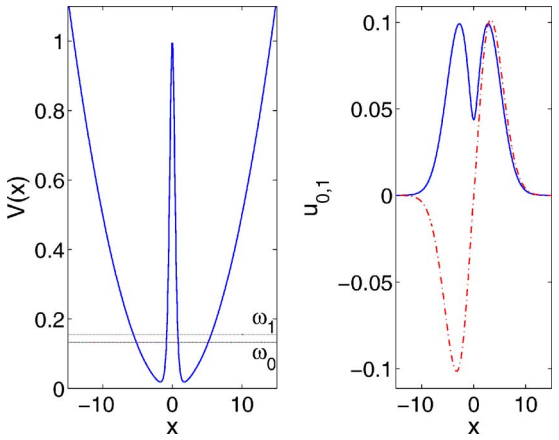

FIG. 1. (Color online) Left panel: The symmetric ($x_0=0$) double-well potential $V(x)$ [see Eq. (2)] with parameters $\Omega=0.1$, $V_0=1$, and $w=0.5$. The horizontal solid lines (ω_0,ω_1) indicate the eigenvalues corresponding to the eigenstates u_0, u_1 of the linear Schrödinger equation ($s=0$). Right panel: The wave functions of the ground state u_0 (blue solid line) and the first excited state u_1 (red dashed-dotted line) for the above double-well potential.

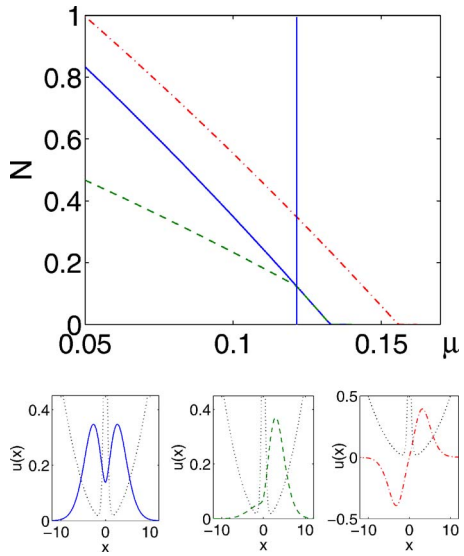

FIG. 2. (Color online) Top panel: The norm of the solutions of Eq. (1) for attractive nonlinearity ($s=-1$) as a function of μ for a symmetric ($x_0=0$) double well. The potential parameters are $\Omega=0.1$, $V_0=1$, and $w=0.5$. The blue solid line denotes the symmetric solution, the red dashed-dotted line denotes the antisymmetric one, while the green dashed line denotes the asymmetric solution that is generated from the bifurcation at $\mu_c\approx 0.122$. Bottom panels: The profiles of the wave functions corresponding to the symmetric (left), asymmetric (middle), and antisymmetric (right) branches for $\mu=0.05$. The black dotted line shows the double-well potential.

that the function u is real if $\phi_{0,1}=k\pi$, with k an integer]. This way, Eq. (6) is automatically satisfied, while Eq. (8) becomes

$$-\Delta\omega + s(A_0\rho_0^2 - A_1\rho_1^2) - 3sB(\rho_0^2-\rho_1^2) = 0. \tag{9}$$

Then, utilizing the definition of the number of atoms $N=\rho_0^2+\rho_1^2$, it is readily found that Eq. (9) leads to

$$\rho_0^2 = \frac{\Delta\omega + sN(A_1-3B)}{s(A_0+A_1-6B)} \tag{10}$$

while, solving Eq. (9) with respect to ρ_1^2, we obtain

$$\rho_1^2 = \frac{\Delta\omega + sN(3B-A_0)}{s(6B-A_1-A_0)}. \tag{11}$$

Let us first consider the case of attractive nonlinearity, i.e., $s=-1$. As the denominator on the right-hand side of Eq. (10) is $6B-A_0-A_1>0$, the numerator has to be non-negative, i.e., $N\geqslant\Delta\omega/(A_1-3B)$. Since the inequality in the latter expression is always true [i.e., for all N, as $\Delta\omega/(A_1-3B)<0$], it is concluded that no solution bifurcates from the antisymmetic branch with $\rho_0=0$. However, Eq. (11) implies that $N\geqslant\Delta\omega/(3B-A_0)$. As the latter requirement can now be satisfied, it is clear that asymmetric solutions, with $\rho_1\neq 0$, can bifurcate from the symmetric ones with $\rho_0^2=N$ and $\rho_1^2=0$. These are the solutions that we are interested in, as they account for the symmetry breaking due to the inclusion of the odd eigenfunction $u_1(x)$ in Eq. (3). To this end, we readily find that the critical value of the norm at which the bifurcation occurs is given by

$$N_c = \frac{\Delta\omega}{3B-A_0}. \tag{12}$$

One can also determine, using Eqs. (4) and (5), the critical chemical potential (propagation constant) at which the symmetry breaking is expected, $\mu_c=\omega_0-A_0N=0.121\,15$. As we will see below, the above analytical predictions are in *excellent* agreement with the numerical results, which, in the case under consideration, are summarized in Fig. 2 (bifurcation diagram) and Fig. 3 (stability diagram).

To construct the bifurcation diagram (Fig. 2), we find numerically the different branches of solutions (including the bifurcating ones) of the time-independent version of Eq. (1) (with $\partial_t u=0$). This is done upon employing a fixed point algorithm (Newton-Raphson) and using the continuation of the solutions for the parameter μ. In the top panel of Fig. 2, with$N$ shown as a function of the chemical potential (or propagation constant in optics) μ. The red dash-dotted branch denotes the antisymmetric solution of Eq. (1); as expected, continuation of this branch to the linear limit ($N\to 0$) shows that it starts (bifurcates) from $\mu=\omega_1$, namely the eigenvalue of the first excited state. The blue solid and green dashed lines correspond, respectively, to the symmetric and asymmetric solutions; the latter bifurcates from the former through symmetry breaking, and the bifurcation point is found to be $\mu_c=0.122(\pm 0.001)$, in excellent agreement with the analytically predicted value ($\mu_c=0.12115$). Note that continuation of the symmetric branch to the linear limit ends with the eigenvalue ω_0, corresponding to the ground state of the linear problem. The bottom panels of Fig. 2 illustrate the profiles of the symmetric (left), asymmetric (middle), and antisymmetric (right) branches for $\mu=0.05$. It is clearly seen that the symmetric and antisymmetric wave functions follow the form of the coresponding linear ones. As far as the asymmetric branch is concerned, we show the one bearing the larger part of the density in the right well (notice that two such asymmetric states arise, being mirror images of each other with respect to the $x=0$ axis).

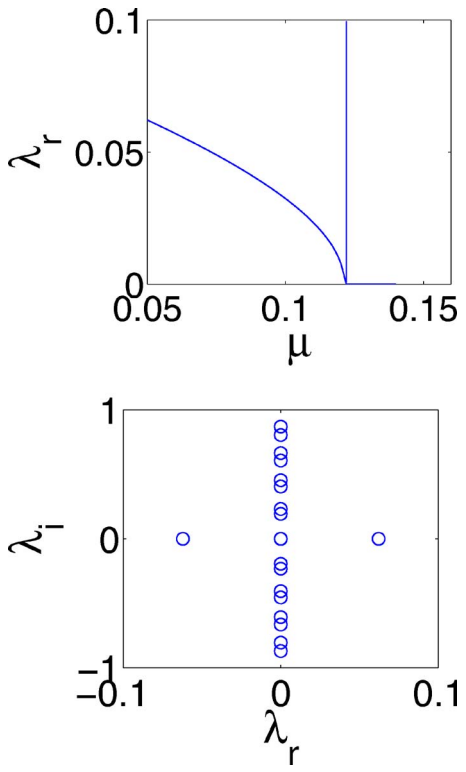

FIG. 3. (Color online) Top panel: The real part λ_r of the most unstable eigenvalue of the symmetric solution as a function of μ; note that the symmetry-breaking bifurcation destabilizes the symmetric solution for $\mu<\mu_c=0.122$. Bottom panel: The result of the linear stability analysis around the symmetric solution for $\mu=0.05<\mu_c$ in the complex plane (λ_r,λ_i). The existence of an eigenvalue with a positive real part implies instability of the solution.

The linear stability of these stationary states, $u_S(x)$, is determined by the eigenvalues λ and eigenvectors (a,b) of the linearized equation, obtained by the substitution of

$$u(x,t)=\{u_S(x)+\epsilon[a(x)e^{\lambda t}+\bar{b}(x)e^{\bar{\lambda}t}]\}e^{-i\mu t} \tag{13}$$

into Eq. (1) and linearization in the formal small parameter ϵ; as the eigenvalues are generally complex, i.e., $\lambda=\lambda_r+i\lambda_i$, instability corresponds to $\lambda_r>0$. The results of the linear stability analysis are shown in Fig. 3. The top panel, displaying the real part λ_r of the most unstable eigenvalue of the symmetric solution as a function of μ, shows that the symmetry-breaking bifurcation destabilizes the symmetric solution (for $\mu<\mu_c=0.122$). This occurs through the appearance of a pair of real eigenvalues, as shown in the bottom panel of Fig. 3 (for $\mu=0.05$) in the complex plane (λ_r,λ_i) of the stability eigenvalues. As the asymmetric solution emerging at the bifurcation point is stable, it is concluded that the bifurcation considered in this case is a (supercritical) *pitchfork*.

Let us now consider the repulsive nonlinearity $(s=+1)$. In this case, as the denominator on the right-hand side of Eq. (10) is $A_0+A_1-6B<0$, the numerator has to be nonpositive, i.e., $N\geqslant\Delta\omega/(3B-A_1)$. The equality in the latter expression can be satisfied, and, thus, the asymmetric solution can bifurcate from the antisymmetic branch with $\rho_0=0$. This way,

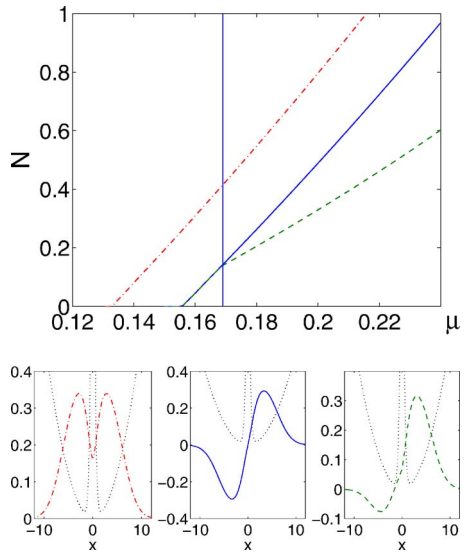

FIG. 4. (Color online) Top panel: Same as in Fig. 2 but for the repulsive nonlinearity $(s=+1)$. The red dashed-dotted line denotes the symmetric solution, the blue solid the antisymmetric one, while the green dashed line corresponds to the asymmetric solution generated from the pitchfork bifurcation occurring at $\mu_c\approx0.168$. Contrary to the case $s=-1$, the bifurcation originates from the antisymmetric branch. Bottom panels: The profiles of the wave functions corresponding to the symmetric (left), antisymmetric (middle), and asymmetric (right) branches for $\mu=0.22$.

the bifurcation does not originate from the symmetric branch but rather from the antisymmetric one, with $(\rho_0,\rho_1)=(0,\sqrt{N})$, giving rise again to symmetry breaking. The critical value of the norm N at which the bifurcation occurs is given by

$$N_c=\frac{\Delta\omega}{3B-A_1}, \tag{14}$$

while the critical value of the chemical potential is $\mu_c=\omega_0+3BN=0.168\,22$. The numerical results are summarized in Fig. 4 (bifurcation diagram) and Fig. 5 (stability diagram). As expected from the above analysis, the asymmetric solution of Eq. (1) emerges from the antisymmetric branch (see the top panel of Fig. 4) through a pitchfork bifurcation. Additionally, Fig. 5 clearly shows that the symmetry-breaking bifurcation destabilizes the antisymmetric solution. (Note that this instability has also been considered and analyzed in Ref. [26]). Moreover, the numerically found critical value of μ where the bifurcation takes place is $\mu_c=0.168(\pm0.001)$, once again in excellent agreement with the analytical result $(\mu_c=0.168\,22)$. Finally, similar to the previous case (pertaining to the attractive nonlinearity), the bottom panels of Fig. 4 illustrate the wave-function profiles for $\mu=0.22$, while the bottom panel of Fig. 5 is a typical example of the linear stability analysis around the unstable antisymmetric solution (for the same value of the chemical potential).

B. Asymmetric double well

Now, we consider the case of an asymmetric double well, assuming a *weak asymmetry* $x_0=0.5$. The form of the double-

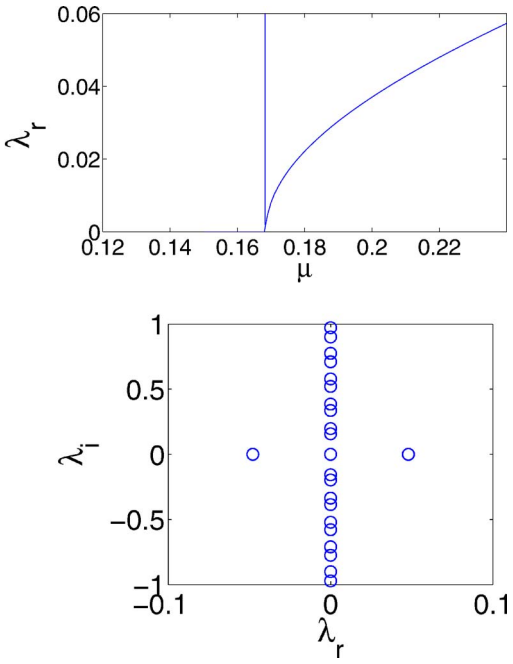

FIG. 5. (Color online) Top panel: The maximal real eigenvalue associated with the linear stability analysis of the antisymmetric-solution branch. Bottom panel: The respective result of the linear stability analysis around the antisymmetric solution when $\mu=0.22 > \mu_{\mathrm{cr}}$ in the complex plane. An eigenvalue with a positive real part implies instability of the solution.

well potential, together with the form of the ground state u_0 and the first excited state u_1 (and the associated eigenvalues) of the corresponding linear problem ($s=0$), are shown in Fig. 6. In this case, the parameters involved in Eqs. (6) and (8) are found to be $A_0=0.149\,03$, $A_1=0.156\,18$, $B=0.029\,58$, $\omega_0=0.1249$, and $\omega_1=0.165\,35$. Additionallly, Γ_0 and Γ_1 are nonzero in the asymmetric case and take the values Γ_0

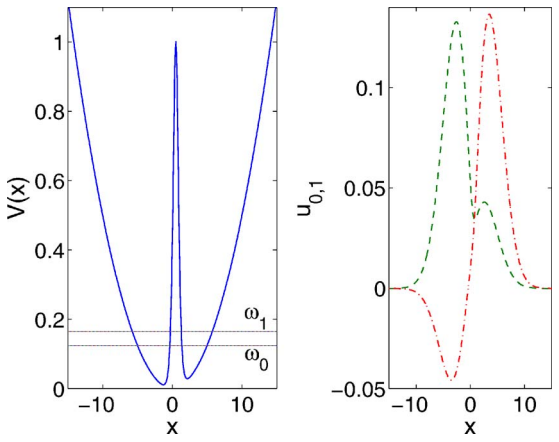

FIG. 6. (Color online) Left panel: The asymmetric double-well potential $V(x)$ [see Eq. (2)] with parameters $\Omega=0.1$, $V_0=1$, $w=0.5$, and $x_0=0.5$. The horizontal solid lines (ω_0,ω_1) indicate the eigenvalues corresponding to the first two eigenstates u_0,u_1 of the linear Schrödinger equation ($s=0$). Right panel: The wave functions of the ground state u_0 (green dashed line) and the first excited state u_1 (red dashed-dotted line) for the above double-well potential.

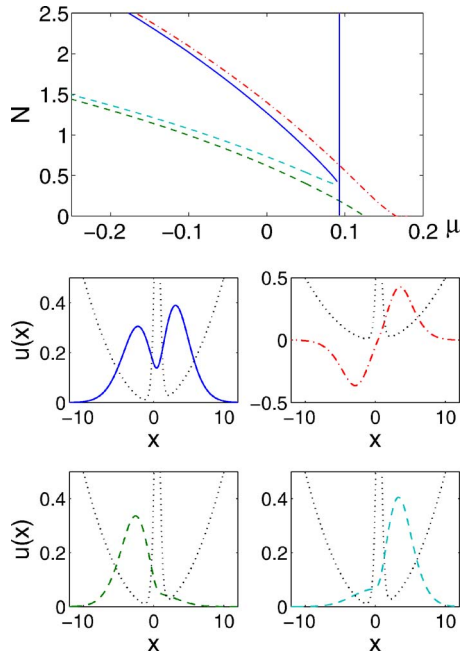

FIG. 7. (Color online) Top panel: The norm of the solutions of Eq. (1) for attractive nonlinearity ($s=-1$) as a function of μ for an asymmetric double well with $x_0=0.5$. The potential parameters are $\Omega=0.1$, $V_0=1$, and $w=0.5$. The lower (green dashed) and upper (red dashed-dotted) branches are the nonlinear continuations (for decreasing μ) of the ground state and the first excited state of the linear problem, respectively; both of these branches end at the linear limit ($N=0$). On the contrary, the remaining two branches in the middle (blue solid line and cyan dashed line) exist up to the critical point $\mu_c\approx 0.09$, where they collide and disappear through a saddle-node bifurcation. Bottom panel: The profiles of the wave functions corresponding to the above-mentioned branches for $\mu=0.05$. The top right (red dashed-dotted) and bottom left (green dashed) solutions are the nonlinear counterparts of the first excited state and the ground state shown in Fig. 6; the top left (blue solid) and bottom right (cyan dashed) solutions are, respectively, the unstable and stable solutions emerging from the saddle-node bifurcation. The black dotted line shows the double-well potential.

$=0.0407$ and $\Gamma_1=-0.040\,77$, respectively. Note that even such a weak asymmetry renders the right well "shallower," in the sense that the norm N of the ground state of the linear problem in the right well is larger than the one in the left well (see the green dashed line in the right panel of Fig. 6).

As far as the nonlinear problem is concerned, we start our analysis considering again first the case of attractive nonlinearity, i.e., $s=-1$. In this setting, it is no longer straightforward to obtain an explicit expression for the critical value of μ (at which the bifurcation occurs) from Eqs. (6)–(8); however, these equations can be easily analyzed with the help of a symbolic mathematical package. Such an analysis predicts a bifurcation to occur at $\mu_c=0.087\,48$. Once again, the respective numerical results summarized in Fig. 7 (bifurcation diagram) and Fig. 8 (stability diagram) are in excellent agreement with the analytical predictions. In particular, the numerically found value of the critical value of μ is $\mu_c=0.09\pm0.001$. Moreover, the analysis reveals also a significant difference between this case and the symmetric case

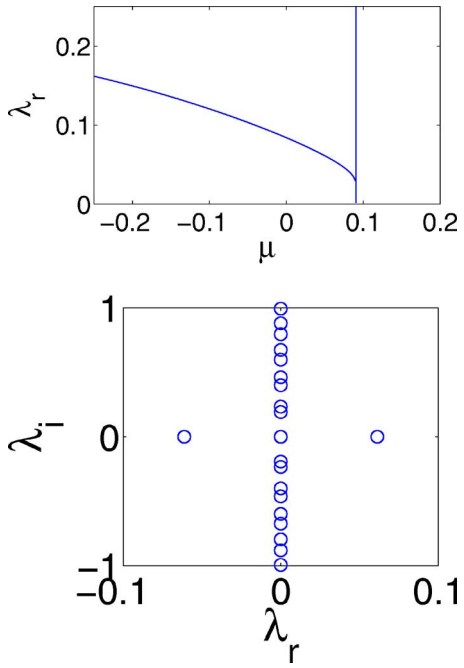

FIG. 8. (Color online) Top panel: The real part λ_r of the most unstable eigenvalue of the "more symmetric" solution as a function of μ; bottom panel: the result of the linear stability analysis around that solution for $\mu=0.05<\mu_c$ in the complex plane (λ_r,λ_i). The existence of an eigenvalue with a positive real part indicates the instability of the solution.

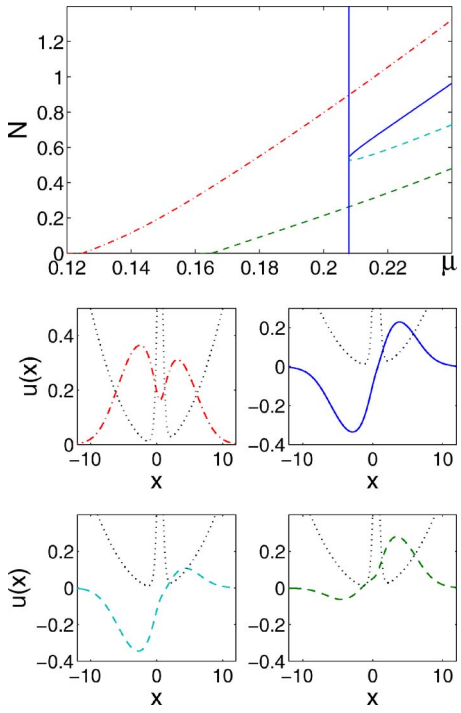

FIG. 9. (Color online) Top panel: Same as in Fig. 7 but for the repulsive nonlinearity ($s=+1$). The upper (red dashed-dotted) and lower (green dashed) branches are the nonlinear continuations (for increasing μ) of the ground state and the first excited state of the linear problem, respectively; both of these branches end at the linear limit ($N=0$). On the contrary, the remaining two branches in the middle (blue solid line and cyan dashed line) exist up to the critical point $\mu_c\approx 0.207$, where they collide and disappear through a saddle-node bifurcation. Bottom panels: The profiles of the wave functions corresponding to the above-mentioned branches for $\mu=0.22$. The black dotted line shows the double-well potential.

discussed above, namely there is no longer a pitchfork bifurcation, but instead, there is a *saddle-node* bifurcation. This result is shown in the top panel of Fig. 7, where N is shown as a function of μ. It is readily observed that, due to the nature of the saddle-node bifurcation, two branches, one of which is stable and the other one is unstable, "collide" at the critical value of $\mu=\mu_c$ and disappear. The unstable branch (see the blue solid line in the top panel, and the respective profile of the wave function for $\mu=0.05$ at the middle left panel) is the more "symmetric" one, which has support on both wells. On the other hand, the stable branch (see the cyan dashed line in top panel, and the respective profile of the wave function for $\mu=0.05$ at the bottom right panel) pertains to a state having the form of a single pulse in the shallower well. The two remaining branches shown on the top panel of Fig. 7, i.e., the lower (green dashed) and upper (red dashed-dotted) ones, are the nonlinear continuations (for decreasing μ) of the ground state and the first excited state of the linear problem, respectively. Notice that both these branches are stable and continue all the way to the linear limit ($N=0$). Finally, it is noted that the result described above, namely the asymmetric breakdown of the pitchfork bifurcation into a saddle-node one, is a *particular feature* of asymmetric double-well potentials, in accordance with general bifurcation theory [24].

The results of the stability analysis for the above-mentioned unstable branch (blue solid line in the top panel of Fig. 7) are shown in Fig. 8. The top panel displays the real part λ_r of the most unstable eigenvalue of the "more symmetric" solution as a function of μ; it is clear that the saddle-node bifurcation makes this solution disappear (for $\mu=\mu_c\approx 0.09$). Prior to this critical point, the solution is unstable due to a pair of real eigenvalues, as shown in the bottom panel of Fig. 8 (for $\mu=0.05$) in the complex plane (λ_r,λ_i) of the stability eigenvalues.

Finally, we consider the case of repulsive nonlinearity ($s=+1$) for the asymmetric potential. Notice that the bifurcation now originates from anti-phase (between the wells) solutions, contrary to the attractive nonlinearity case, where it originated from in-phase solutions. In particular, the branch denoted by the blue solid line in the top panel of the bifurcation diagram of Fig. 9 (see also the profile of the wave function for $\mu=0.22$ in the middle right panel of the same figure) is the unstable one. This branch collides, as previously, with its neighboring one (denoted by the cyan dashed line in the top panel of Fig. 9) at the critical point μ_c and they disappear. Apparently, as we are still dealing with an asymmetric double well, the bifurcation is again of the saddle-node type. The theoretical prediction concerning the value of the critical point where the bifurcation occurs is $\mu_c=0.213\,42$, once again in very close agreement with the numerical result $\mu_c=0.207\pm 0.001$. The details of the bifurcation diagram, and the form of the steady-state solutions, are illustrated in Fig. 9, while their linear stability is shown in Fig. 10.

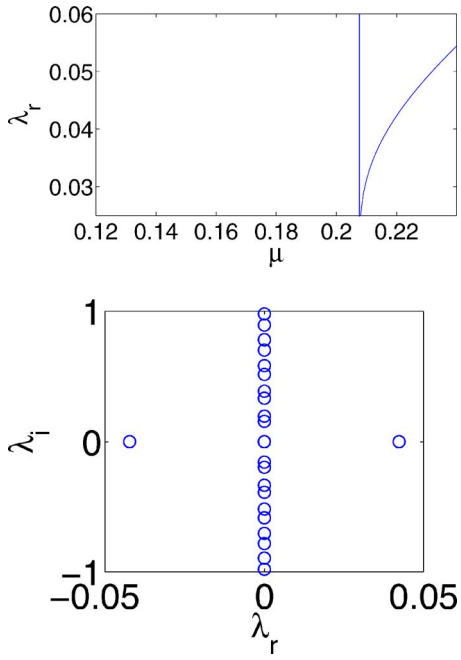

FIG. 10. (Color online) Same as in Fig. 8 but for the repulsive nonlinearity ($s=+1$). Top panel: The real part λ_r of the most unstable eigenvalue of the more "symmetric" solution (as compared to the anti-phase ones—see the middle right panel of Fig. 9) as a function of μ. Bottom panel: The result of the linear stability analysis around this solution for $\mu=0.22>\mu_c$ in the complex plane (λ_r,λ_i).

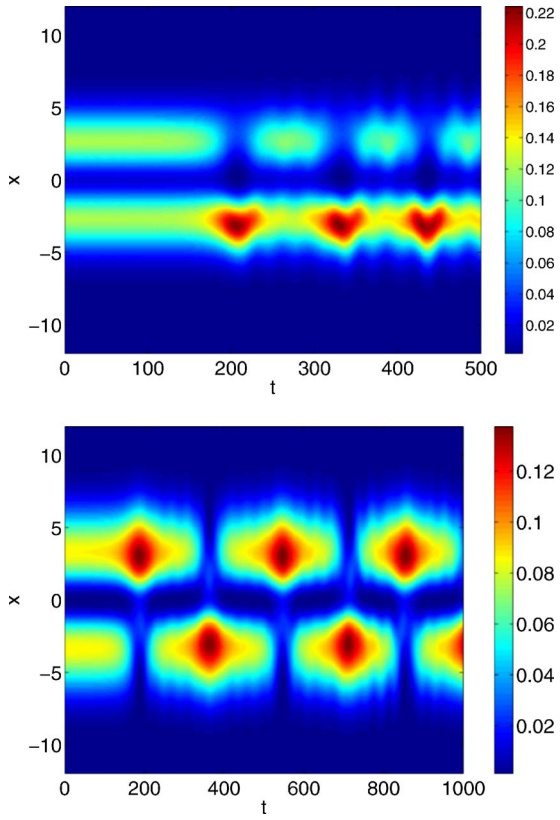

FIG. 11. (Color online) Spatio-temporal countour plot of the density of the unstable solutions in the symmetric double-well potential ($x_0=0$). Top panel shows the evolution of the symmetric solution for the attractive nonlinearity ($s=-1$) and the bottom panel the evolution of the antisymmetric solution for the repulsive nonlinearity ($s=+1$). The potential parameters are the same as in Fig. 1.

IV. DYNAMICS

So far, we have examined the existence, stability, and bifurcations of the branches of solutions in the symmetric or asymmetric double-well problem with attractive or repulsive nonlinearities. For reasons of completeness, we also present the (typical) dynamics of the unstable solutions for each one of the solution branches that were found to be unstable in the above stability computations.

We start with the symmetric double well for the attractive nonlinearity ($s=-1$) and consider the unstable symmetric solution for $\mu=0.05<\mu_c=0.122$ (this solution is also shown in the bottom left panel of Fig. 2). The system is initialized with the exact unstable solution perturbed by a randomly distributed perturbation of amplitude 10^{-4} (in order to accelerate the manifestation of the instability). Its dynamical evolution is shown in the top panel of Fig. 11. As shown in this figure, up to $t\approx 160$ the solution does not change shape, remaining symmetric, but then the instability sets in, resulting in symmetry breaking. This is indicated (for the first time around $t=200$) with a strong accumulation of power (norm) in the right well; then, part of this power is transferred back to the left well (see, e.g., at $t=250$), and so on. Next, we consider (also for the symmetric double well) the case of the repulsive nonlinearity ($s=+1$), shown in the bottom panel of Fig. 11. We now use as an initial condition the unstable antisymmetric solution for $\mu=0.22>\mu_c=0.168$ (also shown in the bottom middle panel of Fig. 4), with an addition of the same type of randomly distributed perturbation as above. Similar to the previous case, after a time interval where the solution remains unchanged (up to $t\approx 200$), symmetry breaking occurs. Then, oscillations are observed, with part of the power being transferred from one well to the other.

Finally, we also consider the dynamical evolution of the unstable solutions of the asymmetric double well (with $x_0=0.5$), both for the attractive ($s=-1$) and repulsive ($s=+1$) nonlinearity. The solution of the former case has a nearly symmetric profile and is found for $\mu=0.05<\mu_c=0.09$ (this wave function is also shown in the middle left panel of Fig. 7); the dynamics of this solution is shown in the top panel of Fig. 12. On the other hand, the solution for the repulsive case corresponds to the nearly antisymmetric branch for $\mu=0.22>\mu_c=0.207$ (see the respective profile of the wave function in the middle right panel of Fig. 9); the evolution of this solution is shown in the bottom panel of Fig. 12. Note that both solutions are initially perturbed by a randomly distributed perturbation as in the previous case. The results of the respective numerical experiments feature again symmetry breaking and occurrence of oscillations as a result of the onset of the instability.

V. CONCLUSIONS

In conclusion, we have presented a systematic analysis based on a Galerkin, two-mode truncation of the stationary

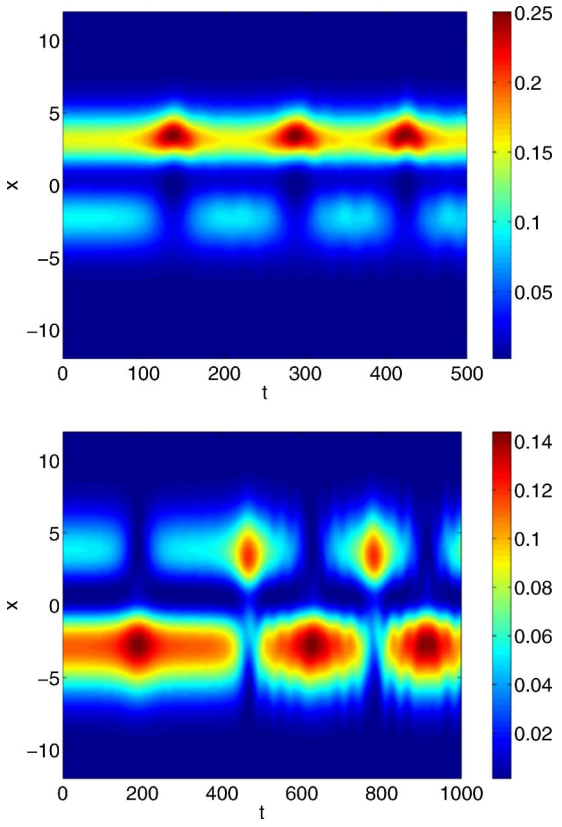

FIG. 12. (Color online) Spatio-temporal countour plot of the density of the unstable solutions in the asymmetric double-well potential ($x_0=0.5$). Top and bottom panels show, respectively, the evolution of the solutions for the attractive ($s=-1$) and the repulsive ($s=+1$) nonlinearity. The potential parameters are the same as in Fig. 6.

states of symmetric and asymmetric double-well potentials. The analysis has been carried out both for repulsive and attractive nonlinearities and, as such, can be relevant to a variety of physical contexts; these include matter-wave physics (most directly), nonlinear optics, as well as other contexts where it is relevant to consider double-well potentials in the NLS model proper. We have demonstrated that our analytical approach describes quite accurately, both *qualitatively* and *quantitatively*, the features of the nonlinear solutions.

In fact, the two-mode analysis used in the present work can successfully be performed in relevant cases of *weakly nonlinear* problems. Particularly, in our case, the bifurcations were found to occur close enough to the linear limit (i.e., for N sufficiently small). Due to the weakly nonlinear nature of the considered problem, our analytical predictions have been found to be in very good agreement with the full numerical results. The agreement was excellent in the case of symmetric potentials and less good in the case of asymmetric ones, due to the fact that the critical values of the chemical potential μ and of the number of particles N are sufficiently far from the linear limit. The accuracy of the analytical prediction for stronger asymmetries can be improved upon incorporating higher-order modes in the asymptotic expansion [see Eq. (3)], which would definitely make the analysis more complex. This issue is indeed a very interesting one, but its detailed investigation is clearly beyond the scope of the present paper.

In the case of a symmetric double-well potential, it has been shown that a symmetry-breaking (pitchfork) bifurcation of the ground state occurs for attractive nonlinearities, while it is absent for repulsive nonlinearities. It has also been found that a similar bifurcation of the first excited state occurs in the relevant branches for repulsive nonlinearities, opposite to the case of attractive ones, where such a bifurcation does not happen. Additionally, regarding the above feature, we have illustrated that symmetric potentials are very particular (degenerate) due to their special characteristic of mirror equivalence of the emerging symmetry-breaking states. We have shown that even weak asymmetries lift this degeneracy and lead to saddle-node bifurcations instead of pitchfork ones that were similarly quantified in both attractive and repulsive nonlinearity contexts. Finally, dynamical simulations of the obtained unstable states were conducted in all cases. The numerical results illustrated that the instability manifests itself as a symmetry breaking, accompanied by subsequent oscillations during which part of the power is transferred from one well to the other.

These results underscore the relevance of analyzing steady-state features of nonlinear models (in the presence of external potentials) based on the states of the underlying linear equations. It would be particularly interesting to examine the extent to which dynamical features of such models can be captured by similar truncations. Such studies are currently in progress and will be reported elsewhere.

ACKNOWLEDGMENTS

Constructive discussions with M. K. Oberthaler are kindly acknowledged. This work has been partially supported from "A.S. Onasis" Public Benefit Foundation (G.T.), the Special Research Account of the University of Athens (G.T. and D.J.F.), and NSF-DMS-0204585, NSF-DMS-0505663 and NSF-CAREER (P.G.K.).

[1] C. Sulem and P. L. Sulem, *The Nonlinear Schrödinger Equation* (Springer-Verlag, New York, 1999).
[2] M. J. Ablowitz, B. Prinari, and A. D. Trubatch, *Discrete and Continuous Nonlinear Schrödinger Systems* (Cambridge University Press, Cambridge, 2003).
[3] F. Dalfovo, S. Giorgini, L. P. Pitaevskii, and S. Stringari, Rev. Mod. Phys. **71**, 463 (1999).
[4] P. G. Kevrekidis and D. J. Frantzeskakis, Mod. Phys. Lett. B **18**, 173 (2004); V. V. Konotop and V. A. Brazhnyi, *ibid.* **18**, 627 (2004).
[5] Yu. S. Kivshar and G. P. Agrawal, *Optical Solitons: From Fibers to Photonic Crystals* (Academic Press, San Diego, 2003).

[6] D. N. Christodoulides, F. Lederer, and Y. Silberberg, Nature (London) **424**, 817 (2003); J. W. Fleischer, J. Fleischer, G. Bartal, O. Cohen, T. Schwartz, O. Manela, B. Freedman, M. Segev, H. Buljan, and N. Efremidis, Opt. Express **13**, 1780 (2005).
[7] S. Raghavan, A. Smerzi, S. Fantoni, and S. R. Shenoy, Phys. Rev. A **59**, 620 (1999); S. Raghavan, A. Smerzi, and V. M. Kenkre, *ibid.* **60**, R1787 (1999); A. Smerzi and S. Raghavan, *ibid.* **61**, 063601(R) (2000).
[8] E. A. Ostrovskaya, Y. S. Kivshar, M. Lisak, B. Hall, F. Cattani, and D. Anderson, Phys. Rev. A **61**, 031601(R) (2000).
[9] K. W. Mahmud, J. N. Kutz, and W. P. Reinhardt, Phys. Rev. A **66**, 063607 (2002).
[10] V. S. Shchesnovich, B. A. Malomed, and R. A. Kraenkel, Physica D **188**, 213 (2004).
[11] D. Ananikian and T. Bergeman, Phys. Rev. A **73**, 013604 (2006).
[12] P. Zin, E. Infeld, M. Matuszewski, G. Rowlands, and M. Trippenbach, Phys. Rev. A **73**, 022105 (2006).
[13] M. Albiez, R. Gati, J. Fölling, S. Hunsmann, M. Cristiani, and M. K. Oberthaler, Phys. Rev. Lett. **95**, 010402 (2005).
[14] C. Cambournac, T. Sylvestre, H. Maillotte, B. Vanderlinden, P. Kockaert, Ph. Emplit, and M. Haelterman, Phys. Rev. Lett. **89**, 083901 (2002).
[15] P. G. Kevrekidis, Z. Chen, B. A. Malomed, D. J. Frantzeskakis, and M. I. Weinstein, Phys. Lett. A **340**, 275 (2005).
[16] E. B. Davies, Commun. Math. Phys. **64**, 191 (1979).
[17] R. K. Jackson and M. I. Weinstein, J. Stat. Phys. **116**, 881 (2004).
[18] R. Khomeriki, J. Leon, and S. Ruffo, e-print nlin.PS/0604045.
[19] W. H. Aschenbacher, J. Fröhlich, G. M. Graf, K. Schnee, and M. Troyer, J. Math. Phys. **43**, 3879 (2002).
[20] T. Kapitula and P. G. Kevrekidis, Nonlinearity **18**, 2491 (2005).
[21] See, e.g., A. Sacchetti, SIAM J. Math. Anal. **35**, 1160 (2004) and references therein.
[22] Y. Shin, M. Saba, T. A. Pasquini, W. Ketterle, D. E. Pritchard, and A. E. Leanhardt, Phys. Rev. Lett. **92**, 050405 (2004); T. Schumm, S. Hofferberth, L. M. Andersson, S. Wildermuth, S. Groth, I. Bar-Joseph, J. Schmiedmayer, and P. Krüger, Nat. Phys. **1**, 57 (2005).
[23] R. Gati, B. Hemmerling, J. Fölling, M. Albiez, and M. K. Oberthaler, Phys. Rev. Lett. **96**, 130404 (2006).
[24] G. Iooss and D. D. Joseph, *Elementary Stability and Bifurcation Theory* (Springer, New York, 1980).
[25] C. Raman, M. Köhl, R. Onofrio, D. S. Durfee, C. E. Kuklewicz, Z. Hadzibabic, and W. Ketterle, Phys. Rev. Lett. **83**, 2502 (1999); R. Onofrio, C. Raman, J. M. Vogels, J. R. Abo-Shaeer, A. P. Chikkatur, and W. Ketterle, *ibid.* **85**, 2228 (2000).
[26] J. A. Stickney and A. A. Zozulya, Phys. Rev. A **66**, 053601 (2002).